ORIGINAL PAPER

Improvement of spatial resolution of elemental imaging using laser ablation-ICP-mass spectrometry

Eisei Tanaka[1] · Takehisa Matsukawa[2,3] · Yasuo Kuroki[4] · Minoru Suzuki[5] · Kazuhito Yokoyama[6,7] · Takafumi Hirata[1]

Abstract

Laser ablation-ICP-mass spectrometer (LA-ICPMS) now becomes one of the most principal analytical technique for mapping analysis for major to trace elements in rocks, minerals, functional materials, or biological tissue samples. In this study, imaging analysis was conducted with coupling of small volume cell and off-set laser ablation protocol to improve the spatial resolution. Combination of newly designed small volume cell and in-torch gas mixing protocols provides faster washout time of the signals (about 0.8 s for reducing ^{238}U being one part in a hundred, 1% level). This is very important to improve the spatial resolution in a direction of laser scanning. Moreover, combination of small distances between the laser-line scan (laser pitch distance) and preferential and total ablation of only biological tissue samples placed on glass substrate results in laser ablation of smaller areas than the size of laser ablation pit (shaving ablation). With the shaving ablation, laser-line scanning with narrower-band width (e.g., 2 μm) can be achieved even by the laser beam of 8 μm diameter. To demonstrate the practical usage of the present technique, imaging analysis of Gd-ethylenediamine tetra-methylene phosphonic acid-doped mouse bone was conducted. Preferential distribution of Gd at the edge of the apatite cell was more clearly identified by the present technique. Combination of the shorter washout system setup and the shaving ablation protocol enables us to improve the spatial resolution of the elemental imaging obtained with the LA-ICPMS technique.

Keywords Laser ablation · ICP mass spectrometry · Imaging · Neutron capture therapy

✉ Takafumi Hirata
hrt1@eqchem.s.u-tokyo.ac.jp

1. Geochemical Research Center, The University of Tokyo, 7-3-1 Hongo, Bunkyo, Tokyo 113-0033, Japan

2. Department of Epidemiology and Environmental Health, Juntendo University, 2-1-1 Hongo, Bunkyo, Tokyo 113-8421, Japan

3. Department of Forensic Science, Juntendo University, Faculty of Medicine, 2-1-1 Hongo, Bunkyo, Tokyo 113-8421, Japan

4. Elemental Group, Thermo Fisher Scientific K.K., 3-9C Kanagawa, Yokohama, Kanagawa 221-0022, Japan

5. Institute for Integrated Radiation and Nuclear Science, Kyoto University, 2 Asashiro-Nishi, Kumatori, Sennan, Osaka 590-0494, Japan

6. Department of Epidemiology and Environmental Health, Juntendo University, Faculty of Medicine, 2-1-1 Hongo, Bunkyo, Tokyo 113-8421, Japan

7. Department of Epidemiology and Social Medicine, Graduate School of Public Health, International University of Health and Welfare, 4-1-26 Akasaka, Minato, Tokyo 107-8402, Japan

Introduction

For imaging analysis, several analytical techniques such as secondary ion mass spectrometry (SIMS), matrix assisted laser desorption/ionization-mass spectrometry (MALDI-MS), or laser ablation-ICP-mass spectrometry (LA-ICPMS) have been widely employed for solid materials. Among them, LA-ICPMS is one of the most sensitive and rapid analytical techniques for measuring spatial distribution of major to trace elements [1, 2]. Ye et al. [3] reported the distribution images of rare earth elements in geological samples. The imaging analysis using the LA-ICPMS technique is now widely used for the trace-element mapping analysis from biological tissue samples [4]. The imaging analyses Mg/Ca and Sr/Ca ratios were conducted on rats-bone samples to evaluate the Ca metabolism [5]. The LA-ICPMS technique can also be applied for the imaging of biomolecules using a tagging technique based on antigen–antibody reaction [6, 7].

Many researchers are increasingly interesting in obtaining further high-spatial resolution images. This is especially true in the study of drug delivery system (DDS), where

distribution analysis of the specific elements or species is highly desired. For the inorganic nutrients, distributions of B or Gd within the cell or tissue samples are gaining attention, since the B and Gd have been widely used for the neutron capture therapy [8]. Detailed distribution analysis of B and Gd is essential to modify chemical forms or status of B and Gd for the DDS studies. In this study, distribution image of Gd was measured from bone tissue samples. Despite the obvious success in obtaining the fast-imaging data from tissue samples, the further detailed distribution feature of Gd is required to understand the mechanism of Gd delivery to the bone tissues. Faced with this, we have tried to improve the spatial resolution of the imaging analysis.

The most plausible approach to improve the spatial resolution is to use the laser ablation with smaller pit sizes. Although higher-spatial resolution images can be derived by laser ablation with 1–2 μm pit sizes, the system must be used the high-magnification lens which results in shallower focusing tolerance. Small changes in focusing condition of the laser beam causes changing in both the drilling rate (i.e., sensitivity) and magnitude of the elemental fractionation during the laser ablation [9]. The laser ablation using the larger beam sizes can largely reduce the source of analytical error originating from these defocusing issuer.

Drescher et al. [10] first reported a new laser ablation protocol to improve the spatial resolution of the elemental imaging. Hence, the laser ablation was achieved only at the front "edge" of the laser beam. The laser ablation was achieved from crescent shaped-ablation pits with width of about 1 μm, resulting in higher-spatial resolution in the direction of laser raster. This approach, however, improves the spatial resolution in one direction, and no improvement can be obtained in the vertical direction of the line scanning. To overcome this, we have developed a new ablation protocol called "shaving ablation" method. In the shaving ablation technique, line-profiling analyses are repeated in the same manner under the conventional line-scanning analysis. Only the difference is the distance between the lines. With the

conventional imaging analysis, distance between the lines is comparable or rather greater than the laser pit size (e.g., 8 μm), whereas the smaller line gap (e.g., 2 μm) is employed for the shaving ablation (Fig. 1).

Another important point to improve the spatial resolution of the resulting elemental imaging data is to shorten the sample washout time. The longer washout time causes after-image toward the scanning direction mainly due to signal tails, resulting in poor spatial resolution of the imaging analysis. Malderen et al. [11] reported the shorter washout time of the signals using a small volume cell. Since the time required for replacing whole gas in the sample cell would be severely dependent upon total volume of the sample cell, the laser induced sample particles can be evacuated from the sample cell. Moreover, the washout time can change by gas flow rates of both the He carrier and Ar make-up gas. In this study, we have tried to improve the spatial resolution of the imaging analysis by combination of (a) small volume cell, (b) optimized addition of the Ar make-up gas, and (c) shaving laser ablation protocol using laser beam with pit size of 8 μm. The main objectivity of this study is to demonstrate that the spatial resolution can be improved without minimizing the laser pit size which can cast off the flexibility and robustness of the laser system.

Experimental section

System setup

The ICPMS system used in this study was a triple-quadrupole based ICPMS (iCAP TQ, Thermo Fisher Scientific, Germany). The laser ablation system was an ultraviolet femtosecond laser equipped with galvanometric scanner (Jupiter Solid Nebulizer, ST Japan INC., Japan). In this study, imaging analysis was carried out based on the repeated line-profiling analysis. Scanning of the laser beam (8 μm in diameter) was conducted by moving the ablation spots by

Fig. 1 Schematic diagram showing the shaving ablation. Sample tissue is ablated by repeated line-scanning laser ablation with a 2 μm off-set which is smaller than the ablation pit size (8 μm). Half-crescent shape area show in black color is newly ablated area
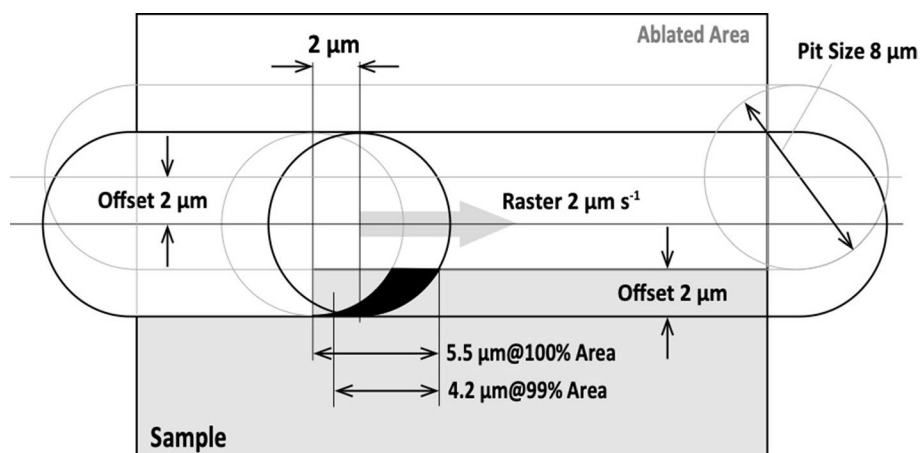
changing the angle of two moving mirrors (Galvanometric optics) equipped on the laser ablation system, and hence, the sample was fixed in position. The repeatability in the positioning of the laser ablation spots, estimated by scanning of laser beam for the maximum sampling area (20×20 mm), is better than 1 μm for 24 h, which is comparable or rather better than those achieved by the conventional laser scanning using electric stages, where small-scale slip of the sample may occur within the cell. The details of instrumental setting are listed in Table 1.

Washout time is key parameter to define both the spatial resolution and analysis time, and the washout time reflects magnitude of spatial spread of the sample particles within the cell or within the transport tubing. Sample particles would be released from the ablation spots and were spread in all directions within the cell, and thus the time required to evacuate all the sample particles would be dependent upon the volume of the cell. This is the main reason why small volume is preferable for the imaging analysis. The sample particles are further spread due to stagnation within the cell and position-dependent flow rate of the transporting gas within the tubing. To minimize the washout time, both the smaller volume of the cell and smaller turbulence within the transport tubing are highly desired. In this study, two approaches were adopted to minimize the washout time. First, newly developed small volume cell (L40 × W20 ×

H5 mm; internal volume 4 mL) instead of conventional cell (L55 × W55 × H5 mm; internal volume 15 mL) was used. Moreover, position of addition of Ar make-up gas was investigated. Because of the large difference in a gas viscosity, uniform mixing of Ar into the He stream is difficult. Incomplete mixing of these gases causes splitting of the He gas stream, resulting in the extension of the time duration of the analyte signals (i.e., lowering the response). To minimize the contribution of extension of signals, gas mixing must be carried out within the high-velocity gas stream. More importantly, after the mixing of the Ar make-up gas, shorter traveling distance is important to minimize spatial diffusion of the sample aerosol onto the Ar. To achieve this, addition of the Ar make-up gas onto the He carrier gas was made through a newly developed mixing chamber (Fig. 2). Hence, mixing of the Ar and He gases was conducted within the injector tubing of the ICP-torch (i.e., only 20 mm before the ICP). In the in-torch mixing, sample aerosols are injected into the ICP with minimum spatial diffusion, and thus, the better signal response can be achieved.

Helium (flow rate of 1.5 L min^{-1}) instead of Ar was used as a carrier gas, and the Ar make-up gas was added to void a lowering the instrumental sensitivity of the LA-ICPMS system. The flow rates of He and Ar gas are important parameters to control both the washout time and transmission efficiency of the ions through the mass

Table 1 Instrumentation and operational conditions

(a) ICP–MS	
Instrument	iCAP TQ (Thermo Fisher Scientific, Germany)
RF power	1550 W
Gas flow rates	Coolant gas: 14 L min^{-1}
	Auxiliary gas: 0.8 L min^{-1}
	He carrier gas: 1.5 L min^{-1}
	Ar make-up gas: 0.7 L min^{-1}
Reaction mode	TQ-O$_2$ mode (O$_2$ reaction gas: 0.25 mL min^{-1})
Monitored isotopes	^{12}C$^+$, ^{31}P$^+$(oxide), ^{157}Gd$^+$(oxide), ^{158}Gd$^+$(oxide)
Dwell time	^{12}C$^+$: 0.1 s
	^{31}P$^+$(oxide), ^{157}Gd$^+$(oxide), ^{158}Gd$^+$(oxide): 0.2 s
(b) Laser ablation system	
Instrument	Jupiter Solid Nebulizer (ST Japan INC., Japan)
Pulse duration	290 fs
Wavelength	260 nm
Fluence	2 J cm^{-2} for tissue sample
	12 J cm^{-2} for glass standard
Repetition rate	100 Hz
Raster speed	10 μm s^{-1} for conventional imaging
	2 μm s^{-1} for shaving ablation protocol
Cell	In-house small volume cell (internal volume 4 mL)
Transport tube	Inside diameter: 3 mm
	Length: 2 m
	Material: polytetrafluoroethylene (PTFE)
Ablation area	300 μm × 200 μm (thickness 5 μm)

Fig. 2 Schematic diagram of sample cell, mixing chamber and ICP-torch
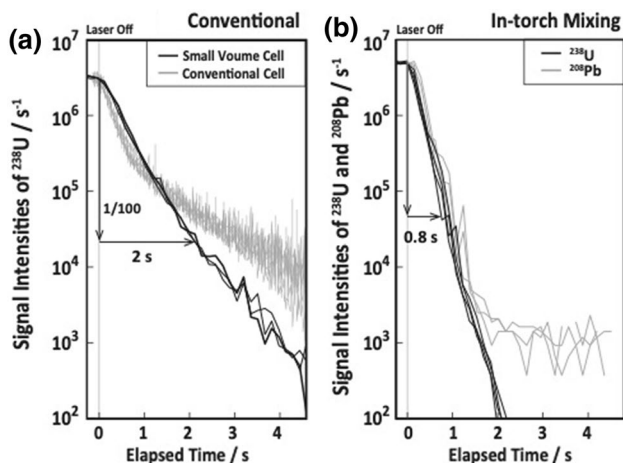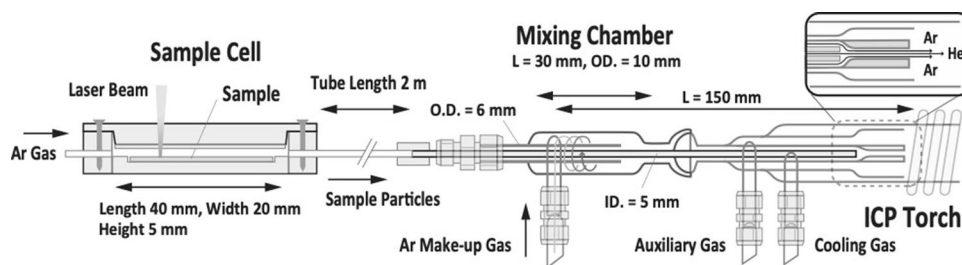
Fig. 3 Comparison of the washout time (defined by signal decay to 1% height) obtained by **a** conventional Ar mixing, and **b** in-torch Ar mixing. The signal decay profiles for the ^{238}U obtained by the conventional sample cell, and the ^{208}Pb obtained by the in-torch mixing technique were also shown in **a** and **b**, respectively

spectrometer. Higher He carrier gas results in faster evacuation of the laser induced sample particles in the cell, but too high He gas flow can cause lowering the signal intensities of analytes, and therefore, He and Ar gas flow rates were carefully optimized to achieve both the higher transmission and short washout time. In this study, flow rates of He and Ar gas were optimized to maximize the transmission of the system, and then flow rate of Ar was optimized to minimizing the washout time. Position of the Ar addition affect the washout time of the signals (defines as time requires signal intensity decays to 1% level after the ending of the laser ablation). Figure 3 illustrates the signal intensity profile of ^{238}U obtained by laser ablation on NIST SRM610 glass material. With the conventional mixing (mixing just after the sample cell), the measured washout time for ^{238}U was about 2 s, whereas the washout time was about 1/3 level (0.8 s) when Ar was added within the injector tubing of the ICP torch. The shorter washout time is effective to reduce the influence of the signal tailing, resulting in better spatial resolution of the imaging analysis, and thus the in-torch mixing was adopted throughout this study. It should be noted that the signal

rise time (defines as time required from the rising edge of the signal to reach a steady signal) could affect the spatial resolution of the imaging analysis. With the LA system setup employed here, the rise time of the ^{238}U signal is about 0.4 s, demonstrating that the rise time is less effective to the spatial resolution of the images.

Sample

The tibia bone sample was collected from female mouse (BALB/cAJcl) of 7-week-old. The animal experiment was approved by the Kyoto University Animal Research Committee and was performed in compliance with the committee guidelines. About 20 mg kg^{-1} of Gd of Gd-EDTMP (ethylenediamine tetra-methylene phosphonic acid) dissolved in phosphate-buffered saline solution was administered to the mouse through an intraperitoneal injection. The mouse was fed and watered ad libitum until 24 h post-dose. After euthanasia the tibia bone was collected. For subsidized to the Gd imaging analysis, the tibia bone was cut into sections 5 μm thickness using the Kawamoto microtome method [12] for subsidized to the Gd imaging analysis. Administrated Gd, together with P as major components of bones were monitored in this study. Hence, oxygen mode was employed to improve the signal-to-background ratio, and the produced PO$^+$ and GdO$^+$ ions were measured with the dwell time of 0.2 s for both.

Among the naturally occurring Gd isotopes, ^{157}Gd has the highest neutron capture cross sections [13, 14], and thus, the distribution of ^{157}Gd is important for the neutron capture therapy based on the Gd. However, ^{158}Gd instead of ^{157}Gd was monitored in this study. This is mainly because that the ^{158}Gd is the most abundant isotope among the naturally occurring Gd isotopes (Isotopic abundance, % of ^{158}Gd: 24.84). Moreover, the isotopic effects found in the Gd isotopes through the most of chemical reactions would be about 1‰ or smaller [15], it is natural to consider that there would be no difference in the resulting distributions between the ^{158}Gd and ^{157}Gd isotopes. In fact, no difference could be found in the resulting images of ^{157}Gd and ^{158}Gd isotopes obtained for bone tissue samples subsidized to the present study.

Results and discussion

Washout time

Washout time was evaluated by the decay profile of the signal intensity of ^{238}U after the turning off the laser. The signal intensity profiles for ^{238}U are given in Fig. 3a. Hence, Ar make-up gas was added just after the cell (conventional setting). The signal intensity profile obtained with the conventional cell (internal volume of 15 mL) was also shown as gray-colored lines in Fig. 3a. Signal decay rate for the first 1 s found in the small volume cell (internal volume 4 mL) was little lower than that found in the conventional cell, and the decay rate for the small volume cell became greater after the 1 s period. The slower decay rate of the signal intensity found on the conventional cell can be explained by the contribution of the stagnation of the gas flow within the cell. The measured washout times were about 2 s for the small volume cell and 3 s for the conventional cell.

For the LA-ICPMS technique, position of addition of Ar make-up gas is also very important to minimize the washout time of the system. With the conventional system setup, Ar make-up gas was added just after the sample cell. This is because that it is believed that the high viscosity gas (Ar) can improve the transport efficiency of the sample particles into the ICP. In this study, the Ar make-up gas was mixed within the injector tubing of the ICP torch (Fig. 2). The signal decay profile for the ^{238}U obtained with the in-torch mixing is given in Fig. 3b. To test the analysis repeatability, data acquisition was repeated three times under the identical conditions. The signal decay profile on ^{238}U demonstrates that the signal decay rate becomes much greater than those found in the conventional system setup. The measured washout time was about 0.8 s, and thus, the spatial spread of the sample particles during the transport can be dramatically minimized. The smaller contribution of the spatial spread of the sample particles can be explained either by the smaller contribution turbulence of He flow within the transport tubing, or by stagnation due to incomplete mixing of Ar and He gas within the transport tubing. Since the viscosity of He gas is lower than that of Ar, magnitude of gas turbulence within the transport tubing could be reduced when only He gas was used. Moreover, when the Ar make-up gas was added within the torch injector, traveling distance of the mixture of Ar and He gas was 30 mm or shorter, and thus the magnitude of spatial spread of the sample particles can be reduced. It is widely recognized that the washout times for the volatile elements such as Ge, Zn, Hg, or Pb can become long [16]. To test this, signal decay profile of ^{208}Pb is also given in gray-colored lines in Fig. 3b. Unlikely with the previous studies, there was no significant difference in the decay rate of the signal intensities between ^{238}U and ^{208}Pb, suggesting that the washout time for both the refractory and volatile elements can be shortened with the present system setup. Because of the shorter washout time, the combination of small volume cell and in-torch mixing protocol was adopted for the imaging analysis.

The analysis sequence begins with the analysis of the carrier gas without any laser ablation (the gas blank), and the C, P, and Gd signal intensities were measured for 30 s. The measured background count rates for ^{12}C, ^{31}P, ^{158}Gd, were 10,000 s^{-1}, 10 s^{-1}, and 10 s^{-1}, and no measured background counts did not vary significantly with the blank intensities obtained by the laser ablation of glass substrate (the ablation blank) [17, 18]. The background measurements were followed by the data acquisition through the laser ablation of tissue samples. After the subtracting the background data from the measured signal intensity data of C, P, and Gd from the tissue samples, signal intensity data were used for both the imaging analysis and concentration analysis. Concentrations of P and Gd in the tissue samples were determined by comparing the signal intensities of P and Gd obtained from the NIST SRM610 glass standard and the volume of material ablated. The concentration values for the P and Gd in the NIST SRM610 are 342.5 ± 53.1 µg g^{-1} [19] and 419.9 ± 25.2 µg g^{-1}, [19] respectively, and the details of the calculation procedures are described in our previous reports. [20].

Shaving ablation

In this study, Gd imaging analyses were conducted by two different ablation protocols. First was an imaging analysis based on repeated-line-profiling analysis using the 8 µm ablation pit. Second approach was imaging analysis based on the shaving ablation protocol described in Fig. 1. Hence, the laser ablation was achieved by the "edge" of laser pits. The half-crescent shape area shown in black color is newly ablated area for time slice of 1 s.

For the shaving ablation, the tissue samples must be ablated completely through the first laser ablation sequence to improve the spatial resolution. Since the residual sample after the first laser ablation sequence can affect to the following ablation, and thus, contributions of the residual analytes released from second and third ablation were carefully investigated. To do this, line-profiling analysis was repeated three times from the identical line area. The signal intensity profiles obtained by the repeated line scanning from identical area were given in Fig. 4. Bone tissue sample was used to test the contribution of Gd signals obtained from second and third ablations. In the first line-profiling analysis, the measured signal intensity of ^{158}Gd varies from 0 to 5000 s^{-1}, reflecting the heterogeneous distribution of Gd within the
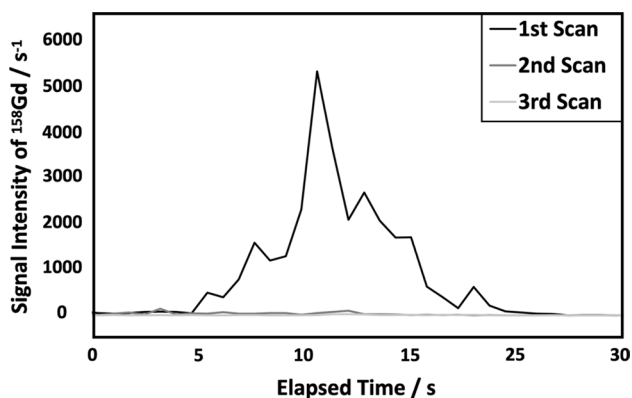
Fig. 4 Signal intensity profiles of Gd obtained by a repeated line profile analysis from identical area of the bone tissue sample

tissue. In the second ablation, the signal intensity of ^{158}Gd became 50 s^{-1}, suggesting the contribution of the sample released from second ablation would be about 1%. With the third laser ablation, the measured signal intensity of ^{158}Gd did not vary measurably from the background counts. The measured Gd signal obtained by the second laser ablation is originating from the residual bone tissues by the first laser ablation sequence. The tissue samples provided for the analysis is about 5 μm in thickness, which is defined by the typical sampling depth for the laser ablation under the present conditions. In this study, fluence and repetition rate of the laser emission was optimized to achieve preferential laser ablation only tissue samples, whereas no laser ablation was made on the glass substrate (i.e., soft ablation protocol) [20]. This is very important to minimize the increase of the background signals originating from the glass substrates. Energy threshold for the laser ablation of glass material (about 7 J cm^{-2} with Ti:S femtosecond laser) is higher than those for biological tissues (about 3 J cm^{-2}), and thus, the fluence of 4–5 J cm^{-2} was adopted for preferential laser ablation only for the biological tissues [8]. Under these conditions, a drilling rate for the bone samples would be lower than those for other parts (e.g., organelles or cell wall), and small portion of the bone samples (e.g., 1%) still remains on the glass substrate even after the first laser ablation sequence. The repeated line-profiling analysis on the identical position revealed that the contribution of Gd from residual bone tissues would not be greater than 1%.

Imaging analysis

For the visualization of the elemental images, time-dependent signal intensity profile was converted to position-based signal intensity profile based on the raster speed and elapsed time using the in-house software "XQuant" modified from the iQuant2 [5, 20, 21]. Figure 5a is a photographic image of the sample before ablation. Fig. 5b and c are color images
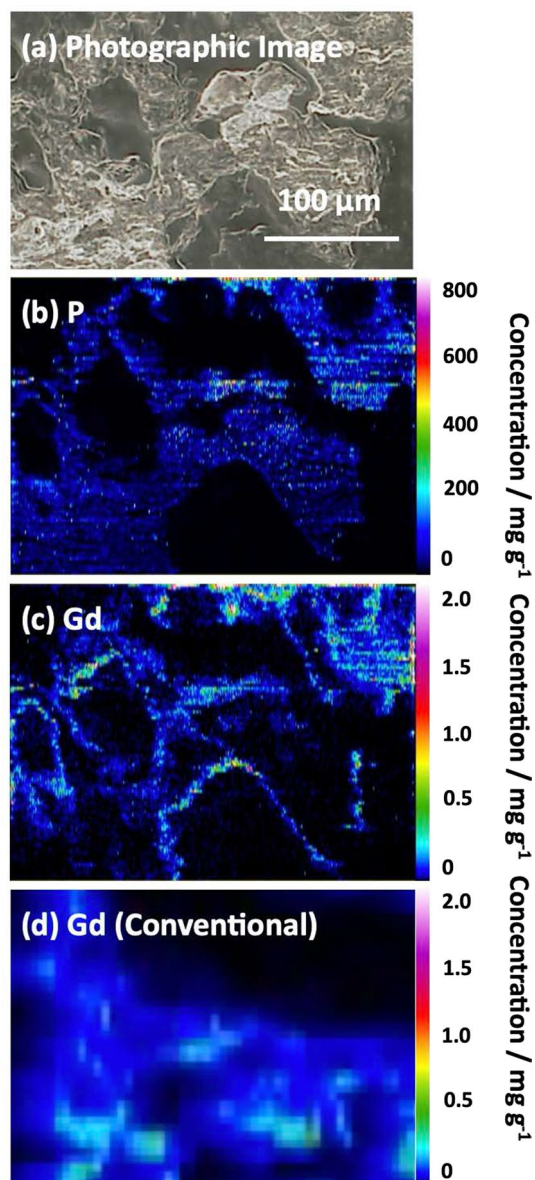
Fig. 5 Photographic and the resulting elemental images for P and Gd: **a** photographic image, **b** P, **c** Gd, and **d** Gd obtained by conventional line-scanning analysis

based on signal intensities of ^{31}P and ^{158}Gd respectively. For comparison of resolution, the Gd image was also obtained by the conventional line-profiling analysis (Fig. 5d).

Figure 5b illustrates the resulting image of P as a major component of bone, suggesting that distribution of P is well consistent with morphology of the bone tissue. In contrast, Gd image (Fig. 5c) shows that the administered Gd is preferentially distributed at the edge of bone. Measured concentrations based on the simple assumption that the mean density of bone was 2 g mL^{-1}, varied 100–200 mg g^{-1} for P (Fig. 5b) and 0–1.5 mg g^{-1} for Gd (Fig. 5c). Concentration range of P in the bone tissue is consistent with the reported

value (ca. 180 mg g^{-1}) [22]. The Gd peak concentrations at the edge of the bone tissue exceeded 0.5 mg g^{-1}, whereas the averaged Gd concentration at middle of the bone tissues was 0.2 mg g^{-1} or less, demonstrating the preferential enrichment of Gd at the edge of the bone tissues. For comparison, Gd image obtained based on the conventional line-scanning analysis using the laser pits of 8 μm was given in Fig. 5d. The peak concentration of Gd at the edge of the bone tissues were about 0.2–0.4 mg g^{-1} (Fig. 5d), suggesting that the concentration range of the Gd was significantly lower than those found in the shaving protocol (Fig. 5c). The slightly lower Gd concentrations found in the conventional imaging analysis can be due to moderation of the Gd contents through a dilution with the low-Gd components. The concentration data obtained here suggested that the measured concentration values can be lowered if in the case that the analytes are concentrated into small areas. Despite this, the imaging data obtained here demonstrates clearly that the further precise discussion for the locations and level of enrichments can be made by the imaging with the present shaving technique, and the resulting distribution features and the concentration ranges of the analytes can be useful to evaluate the toxicity of the elements, or to optimize the size of the administration (dosage).

Spatial resolution

For the imaging analysis, a spatial resolution can be defined as a minimum spacing (Δx) required to separate two areas having equal signal intensities. In the case of mass spectrometer, the mass resolution of the spectrometer (R) is defined as the reciprocal of the mass difference at mass m in unified atomic mass units ($\Delta m/m$), and the Δm is the amount by which the mass of another peak of equal intensity can be separated. The Δm is the width of the peak at 5% or 1% peak height level in unified atomic mass unit. In this study, according to the practical definition of the mass resolution, spatial resolution is defined by the minimum spacing (Δx) based on the traveling distance for the signal decay to 1% peak height level.

Based on the signal intensity profile, the time required for the signal decay down to 1% peak height level is about 0.8 s obtained by the present system setup (Fig. 3b). Since the laser scan rate employed here is 2 μm s^{-1}, the calculated minimum traveling is 1.6 μm. This is satisfactory level for the most of imaging analysis. However, the practical spatial resolution of the imaging analysis defined by the minimum distance (Δx) is deteriorated due to the shape of laser ablation pit obtained by the shaving protocol (Fig. 1). With the shaving ablation, the resulting shape of the ablation area becomes a half-crescent shape with 5.5 μm length with 2 μm width (Fig. 1). This suggests that the sample particles released from elongated positions covering 5 μm was mixed

and averaged, resulting in a lowering the spatial resolution. However, since the rear-part of the half-crescent shape has sharp edge, mass fraction released from sharp-edge area would be low. Based on the geometrical calculations, 99% mass of samples are released from half-crescent area with the length of 4.2 μm (Fig. 1). This suggests that the 99% mass of sample particles are released from area with 4 μm in scan-direction and 2 μm width, demonstrative of nearly doubled better spatial resolution can be obtained by the shaving ablation protocol. Although the magnitude of the improvements in the resulting spatial resolution is limited, it should be noted that spatial resolution can be improved when the small laser pit size (e.g., 5 μm or 2 μm) was used. As mentioned in earlier section, great care must be placed for both the defocusing of the laser beam due to shallower focusing depth and larger elemental fractionation due to high-aspect ratio of the ablation pits. With the present shaving ablation protocol, spatial resolution of the elemental imaging can be improved with keeping the quantitative capability of the system. The technique develop here can become a useful tool to improve the spatial resolution of the imaging analysis.

Conclusive remarks

Imaging analysis was carried out by the ICPMS technique equipped with UV femtosecond laser ablation system. Combination of in-torch mixing of Ar make-up gas and use of in-house small volume cell (internal volume of 4 mL) resulted in shorter washout time of the ^{238}U signal (0.8 s at 1% intensity of original signal). This is very important to improve the spatial resolution of the system.

In this study, newly developed shaving ablation protocol was employed to improve the spatial resolution of the images. Hence, the signal line profiles were obtained by repeated line-scanning analysis with smaller distances between the lines (i.e., 2 μm). This suggests that laser ablation was achieved only 2 μm width using the "edge" of the laser pit. To minimize the contribution of the signals originating from the residues of the previous laser sampling, the bone tissue samples with 5 μm thickness was nearly completely ablated with the first laser scanning. The measured contribution of the second laser ablation was not greater than 1%. Important feature of the present shaving technique is that the system is less susceptible to the changes of the drilling rate or magnitude of elemental fractionation due to defocusing effect originating the rough surface of the sample.

The spatial resolution of the present system setup and analysis protocols was defined by the minimum distance to two sample points with equal signal intensities. The resulting spatial resolution obtained by the laser pit size of 8 μm was 4.2 μm in scanning direction and 2 μm in vertical direction. The improvement of the spatial resolution was well

demonstrated by the Gd imaging for tibia bone samples collected from mouse. The laser optics for 8 μm pit sizes would be much more simple or robust than the system for the laser ablation pit of 2 μm or 4 μm, and thus, the bottom line of this study is that the present analytical protocol can become a major approach to obtain spatial resolution of about 4 μm with the laser pit size of 8 μm.

Another important feature achieved by the shaving technique is the quantitative capability for the analytes. The abundance values were obtained by calibration using the NIST standard glass material based on comparison of signal intensity and ablated volume. In this study, imaging analysis of Gd was conducted on the 5 μm thick sample. Measurements of thicker samples or samples with different matrix would require higher fluence or higher repetition rate. Hence, it is important to confirm whether a sample is completely ablated before conducting shaving ablation protocol. Abundance values with higher-spatial resolution imaging data can be useful information to understand the scientific insights in both the geochemistry and biochemistry.

Declarations

Conflict of interest There are no conflicts to declare.

References

1. J.S. Becker, *Inorganic Mass Spectrometry: Principles and Applications* (Wiley, Chichester, 2007)
2. J.S. Becker, M. Zoriy, J.S. Becker, J. Dobrowolska, A. Matusch, J. Anal. At. Spectrom. **22**, 736 (2007)
3. Y. Ye, H. Wang, X. Wang, L. Zhai, C. Wu, S. Zhang, Palaeogeogr. Palaeoclimatol. Palaeoecol. **538**, 109459 (2020)
4. S. Shimma, Y. Makino, K. Kojima, T. Hirata, Mass Spectrom. **9**(1), A0086 (2020). https://doi.org/10.5702/massspectrometry.A0086
5. Y. Tanaka, N. Yajima, M. Okada, T. Matsumoto, Y. Higuchi, S. Miyazaki, H. Yamato, T. Hirata, Analyst **142**, 4256 (2017)
6. D. Pozebon, G.L. Scheffler, V.L. Dressler, J. Anal. At. Spectrom. **32**, 890 (2017)
7. B. Neumann, S. Hösl, K. Schwab, F. Theuring, N. Jakubowski, J. Neurosci. Methods **334**, 108591 (2020). https://doi.org/10.1016/j.jneumeth.2020.108591
8. W. Lee, K. Jung, J. Park, J.Y. Kim, Y.J. Lee, Y. Chang, J. Yoo, Biochem. Biophys. Res. Commun. **568**, 23 (2021)
9. T. Hirata, R.W. Nesbitt, Geochim. Cosmochim. Acta **59**, 2491 (1995)
10. D. Drescher, C. Giesen, H. Traub, U. Panne, J. Kneipp, N. Jakubowski, Anal. Chem. **84**(22), 9684 (2012)
11. S. Malderen, A.J. Managh, B.L. Sharpb, F. Vanhaecke, J. Anal. At. Spectrom. **31**, 423 (2016)
12. T. Kawamoto, Arch. Histol. Cytol. **66**, 123 (2003)
13. R.K. Adair, Rev. Mod. Phys. **22**, 249–289 (1950)
14. R. B. Firestone, V. S. Shirley, in *Table of Isotopes*, ed. R. B. Firestone, V. S. Shirley, 8th ed., [157]Gd, (Wiley, New York, 1996), pp. 1716–1719
15. J. Bigeleisen, M.G. Mayer, J. Chem. Phys. **15**, 261 (1947)
16. T. Hirata, R.W. Nesbitt, Geochim. Cosmochim. Acta. **59**, 2491–2500 (1995)
17. T. Iizuka, T. Hirata, Geochem. J. **38**, 229–241 (2004)
18. S. Sakata, K. Hattori, H. Iwano, T.D. Yokoyama, T. Danhara, T. Hirata, Geostand. Geoanal. Res. **38**, 409–420 (2014)
19. N.J.G. Pearce, W.T. Perkins, J.A. Westgate, M.P. Gorton, S.E. Jackson, C.R. Neal, S.P. Chenery, Geostand. Newslett. **21**, 115–144 (1997)
20. Y. Makino, S. Ohara, M. Yamada, S. Mukoyama, K. Hattori, S. Sakata, Y. Tanaka, T. Suzuki, A. Shinohara, T. Matsukawa, K. Yokoyama, T. Hirata, in *Metallomics*, (Springer, Tokyo, 2017), pp. 93–106.
21. T. Suzuki, S. Sakata, Y. Makino, H. Obayashi, S. Ohara, K. Hattori, T. Hirata, Mass Spectrom. **7**, 3 (2018)
22. C. M. Weaver in *Present Knowledge in Nutrition*, ed. B. A. Bowman, R. M. Russel, 8th ed., (ILSI Press, Washington DC., 2001), pp. 273–280